

CHAPTER 4

SORET AND DUFOUR IMPACT ON MHD WILLIAMSON
FLUID FLOW WITH VARYING VISCOSITY

Content of this chapter is communicated.

Chapter 4

Soret and Dufour impact on MHD Williamson fluid flow with varying viscosity

Williamson fluid is characterized as a non-Newtonian fluid with shear thinning property i.e., viscosity decreases with increasing rate of shear stress. Chyme in small intestine is one of the example of Williamson fluid. The temperature of the fluid as well as the nature of the fluid have a major impact on viscosity. The viscosity should be a temperature dependant variable rather than a constant at high temperatures. When calculating the surface calculating factors, the assumption of constant viscosity causes measurably inaccurate results.

4.1 Introduction of the Problem

Industrial and scientific processes rely heavily on non-Newtonian fluids, it compel researchers to investigate the phenomena of heat and mass movement. Human blood, shampoos, pulps, honey, sugar, jelly, and other non-Newtonian fluids fall into this category. Williamson fluid falls into pseudo-plastic category. Photographic films, blood cells, food processing, and inkjet printing are just a few of the applications for pseudo-plastic fluids in engineering and industry. In this research, we have taken the constitutive equation known as the Williamson model by Williamson [110]. Nadeem et al. [123] scrutinized 2D flow of Williamson fluid model past stretching sheet.

Natural convection flow happens much of the time in nature. It happens because of positive temperature contrasts, as well as because of concentration contrasts or the combination of these two. Natural convection has broad applications, like, in the plan of the nuclear reactor, digital gear cooling, insulation of plane cabin, and manage of heating and air flow in constructing design, and so on. The Boussinesq

models are utilized to show this angle. In the Boussinesq guess, density changes with temperature difference. Effect of Natural convection on various MHD liquid stream with different geometries have been discussed by Wang et al. [136] and Gireesha and Roja [20].

Influence of Soret and Dufour effects have notable fascination among numerous scientists inferable from different developed designing applications, for example, fabricate for elastic and plastic sheets, chemical creation designing, geophysical cycles, Catalytic interaction, compact heat insulation exchangers and plan of atomic reactor. A lot of examination work has been done to show the significance of dissemination thermo and warm dispersion and impacts for the various viewpoints. Radiation effects on MHD non-Newtonian fluids over vertical plate with Soret and Dufour effects have been found by Huang [26]. Pal et al. [28] scrutinized MHD fluid flow with heat and mass transfer over a vertical stretching sheet considering Soret and Dufour effects. Bég et al. [101] examined the Soret and Dufour effects on MHD fluid flow from a vertical stretching surface. Later, Chamkha and Rashad [8] studied MHD fluid flow with heat and mass transfer in the presence of magnetic field, Soret and Dufour effects.

In the assembling enterprises, radiative heat transfer assumes a crucial part for gas cooled atomic gadgets for between inter-terrestrial flight, the plan of steel rolling, programme of fins, gas turbines, rockets, underground atomic garbage removal and advancements in hypersonic flights, and so on. Rashidi et al. [85] explored significance of radiation on 2D steady MHD fluid flow with free convective mass and heat exchange. Effect of linear thermal radiation on MHD liquid flow have been scrutinized by Mehta and Kataria [108].

4.2 Novelty of the Chapter

To the best of the knowledge, till date there are no attempts to model, no investigation has been made which provides the analytic expression for the steady two-dimensional MHD Williamson fluid flow over stretching sheet considering the effect of heat generation/absorption, nonlinear radiation and variable viscosity. Homotopy analysis method [120] is used for finding solutions of the governing equations.

4.3 Mathematical Formulation of the Problem

Figure 4.1 shows incompressible MHD Williamson fluid flow past a stretching sheet. It is assumed that the sheet is stretching with the plane $y = 0$ and that the flow

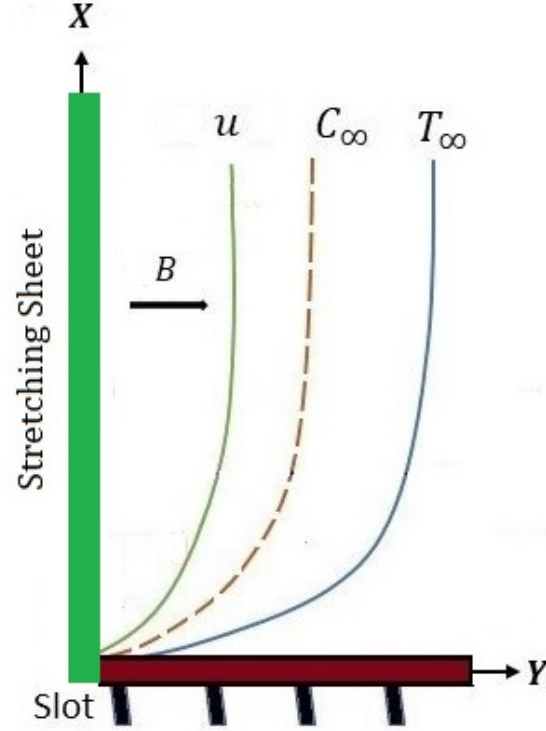


Figure 4.1: Physical problem

is constrained to $y > 0$. In the scenario where $a > 0$ is constant and the x -axis is estimated along the extending surface, with stretching velocity $u(x) = ax$. A uniform magnetic field that is applied perpendicular to an expanding sheet.

The governing equations for Williamson fluid are:

$$\nabla \cdot V = 0 \quad (4.3.1)$$

$$\rho \frac{dV}{dt} = \nabla \cdot S + F_L + \rho \{g\beta_C(C - C_\infty) + g\beta_T(T - T_\infty)\} \quad (4.3.2)$$

$$\rho C_p \frac{dT}{dt} = \nabla \cdot (\kappa \nabla T) + Q^*(T - T_\infty) - \nabla q_r + \nabla \cdot \left\{ \frac{\rho D_M K_T}{C_s} \right\} \nabla C \quad (4.3.3)$$

$$\frac{dC}{dt} = \nabla \cdot \{D_M \nabla C\} + \nabla \cdot \left\{ \frac{D_M K_T}{T_m} \nabla T \right\} \quad (4.3.4)$$

where V is velocity vector and $\frac{d}{dt}$ represents material time derivative.

The governing equations for Williamson fluid are:

$$\frac{\partial u}{\partial x} + \frac{\partial v}{\partial y} = 0, \quad (4.3.5)$$

$$u \frac{\partial u}{\partial x} + v \frac{\partial v}{\partial y} = \frac{1}{\rho} \frac{\partial}{\partial y} \left(\mu(T) \frac{\partial u}{\partial y} \right) + \frac{\Gamma}{\sqrt{2}\rho} \frac{\partial}{\partial y} \left[\mu(T) \left(\frac{\partial u}{\partial y} \right)^2 \right] - u \frac{\sigma B^2}{\rho} + g\beta_C(C - C_\infty) + g\beta_T(T - T_\infty), \quad (4.3.6)$$

$$u \frac{\partial T}{\partial x} + v \frac{\partial T}{\partial y} = \frac{\kappa}{\rho C_p} \frac{\partial^2 T}{\partial y^2} + \frac{\rho D_M K_T}{C_s} \frac{\partial^2 C}{\partial y^2} + Q^*(T - T_\infty) - \frac{1}{\rho C_p} \frac{\partial q_r}{\partial y}, \quad (4.3.7)$$

$$u \frac{\partial C}{\partial x} + v \frac{\partial C}{\partial y} = \frac{D_M K_T}{T_m} \frac{\partial^2 T}{\partial y^2} + D_M \frac{\partial^2 C}{\partial y^2}, \quad (4.3.8)$$

with

$$u = U_w = ax, \quad v = 0, \quad C = C_w, \quad T = T_w \text{ at } y = 0, \quad (4.3.9)$$

$$u \rightarrow 0, \quad C \rightarrow C_\infty, \quad T \rightarrow T_\infty \text{ at } y \rightarrow \infty. \quad (4.3.10)$$

Linearized Heat flux [126] is:

$$q_r = -\frac{16\sigma^*}{3k^*} T_\infty^3 \frac{\partial T}{\partial y} \quad (4.3.11)$$

For the significance of non-linear thermal radiation, we convert T_∞^3 with T^3 in the equation (4.3.11),

$$q_r = -\frac{16\sigma^*}{3k^*} T^3 \frac{\partial T}{\partial y} \quad (4.3.12)$$

then,

$$\frac{\partial q_r}{\partial y} = -\frac{16\sigma^*}{3k^*} \left[3T^2 \left(\frac{\partial T}{\partial y} \right)^2 + T^3 \frac{\partial^2 T}{\partial y^2} \right] \quad (4.3.13)$$

The temperature dependent viscosity by Ajayi et al. [127] is

$$\mu(T) = \mu^* [1 + b(T_w - T)], \text{ where } b > 0. \quad (4.3.14)$$

Introducing the following transformation to convert equations (4.3.5)-(4.3.10),

$$\psi = x\sqrt{a\nu}f(\eta), \quad \eta = \sqrt{a/\nu}y, \quad u = axf'(\eta), \quad v = -\sqrt{a\nu}f(\eta), \quad (4.3.15)$$

$$C = C_\infty + (C_w - C_\infty)\phi(\eta), \quad T = T_\infty + (T_w - T_\infty)\theta(\eta). \quad (4.3.16)$$

Using above transformations, equations (4.3.6-4.3.10) become :

$$(1 + \zeta - \zeta\theta) f''' (1 + 2We f'') - \zeta (1 + We f'') f''\theta' + ff'' - Mf' + Gr_T\theta + Gr_C\phi - f'f' = 0 \quad (4.3.17)$$

$$\left(1 + \frac{4}{3}Rd\{1 - (1 - \theta_w)\theta\}^3\right) \theta'' + 4Rd\{(1 - \theta_w)\theta - 1\}^2(1 - \theta_w)\theta'^2 + DuPr\phi'' + \beta Pr\theta + Prf\theta' = 0 \quad (4.3.18)$$

$$\phi'' + Sc\phi'f + SrSc\theta'' = 0 \quad (4.3.19)$$

with

$$f(0) = \phi(\infty) = f'(\infty) = \theta(\infty) = 0, \quad f'(0) = \phi(0) = \theta(0) = 1. \quad (4.3.20)$$

where $\beta = \frac{Q^*}{a\rho C_p}$, $Pr = \frac{\mu C_p}{k}$, $\zeta = b(T_w - T_\infty)$, $M = \frac{\sigma B^2}{\rho a}$, $Sc = \frac{\nu}{D_M}$, $We = \sqrt{\frac{\Gamma^2 a^3 x^2}{2\nu}}$, $Sr = \frac{D_M K_T (T_w - T_\infty)}{\nu T_m (C_w - C_\infty)}$, $\theta_w = \frac{T_w}{T_\infty}$, $Rd = \frac{4\sigma^* T_\infty^3}{k^* \kappa}$, $Gr_C = \frac{g\beta_C (C_w - C_\infty)}{a^2 x}$, $Du = \frac{D_M K_T (C_w - C_\infty)}{\nu C_s C_p (T_w - T_\infty)}$ and $Gr_T = \frac{g\beta_T (T_w - T_\infty)}{a^2 x}$.

Skin friction factor, rate of heat and mass transfer at the wall are respectively

$$C_f = \frac{\tau_w}{\rho U_w^2}, \quad Nu = \frac{xq_w}{\kappa(T_w - T_\infty)}, \quad Sh = \frac{xq_m}{D_M(C_w - C_\infty)} \quad (4.3.21)$$

At the wall, τ_w , q_m and q_w denote the skin stress, diffusion of mass and heat, where τ_w , q_m and q_w defined in the following

$$\tau_w = \mu u_y [1 + \Gamma u_y]_{y=0}, \quad q_m = -D_M [C_y]_{y=0}, \quad q_w = -\kappa \left(1 + \frac{16\sigma^* T^3}{3k^* \kappa}\right) [T_y]_{y=0}. \quad (4.3.22)$$

using similarity variables, Skin friction factor, Sherwood and Nusselt numbers

$$\left. \begin{aligned} C_f \left(Re_x^{\frac{1}{2}}\right) &= (1 + \zeta - \zeta\theta) f''(0) [1 + We f''(0)], \\ Sh Re_x^{-\frac{1}{2}} &= -\phi'(0), \quad Nu Re_x^{-\frac{1}{2}} = -\left(1 + \frac{4}{3}Rd\{1 + (\theta_w - 1)\theta\}^3\right) \theta'(0), \end{aligned} \right\} \quad (4.3.23)$$

where $Re_x^{\frac{1}{2}} = \sqrt{\frac{\rho}{\mu}} x$.

4.4 Solution by Homotopy Analysis Method

Initial guesses and auxiliary linear operators are respectively

$$f_0(\eta) = 1 - e^{-\eta}, \quad \theta_0(\eta) = e^{-\eta}, \quad \phi_0(\eta) = e^{-\eta}, \quad (4.4.1)$$

$$\mathcal{L}_f = \frac{\partial^3 f}{\partial \eta^3} - \frac{\partial f}{\partial \eta}, \quad \mathcal{L}_\theta = \frac{\partial^2 \theta}{\partial \eta^2} + \frac{\partial \theta}{\partial \eta}, \quad \mathcal{L}_\phi = \frac{\partial^2 \phi}{\partial \eta^2} + \frac{\partial \phi}{\partial \eta}, \quad (4.4.2)$$

with $\mathcal{L}_f(k_1 + k_2e^\eta + k_3e^{-\eta}) = 0$, $\mathcal{L}_\theta(k_4 + k_5e^{-\eta}) = 0$, $\mathcal{L}_\phi(k_6 + k_7e^{-\eta}) = 0$, where $k_i, i = 1, 2, \dots, 7$ are arbitrary constants.

4.4.1 Convergence Analysis

Solutions for HAMs are highly dependent on values for auxiliary parameters \hbar_f , \hbar_θ and \hbar_ϕ that influence convergence and approximation rates. As a result, the Figures 4.2, 4.3 and 4.4 show corresponding \hbar -curves taking 20th HAM approximation. For the values $\hbar_f = -1.09$, $\hbar_\theta = -0.75$ and $\hbar_\phi = -0.83$, we get convergence of the series, which is represented through Table 4.1.

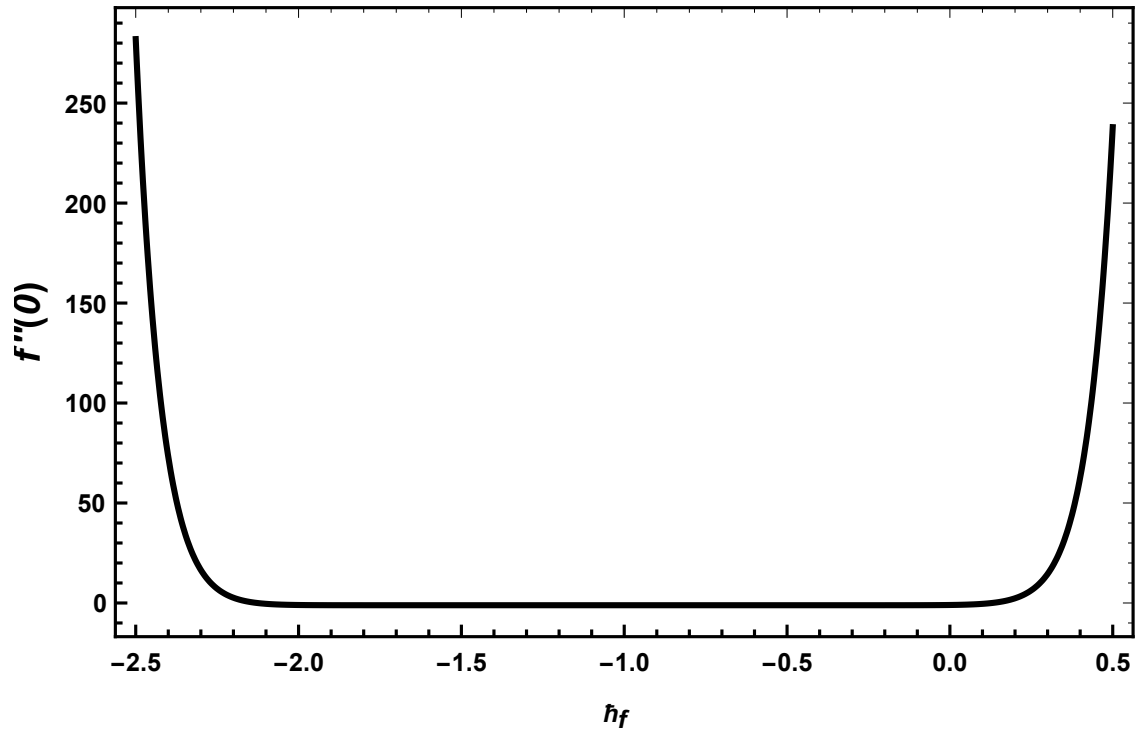
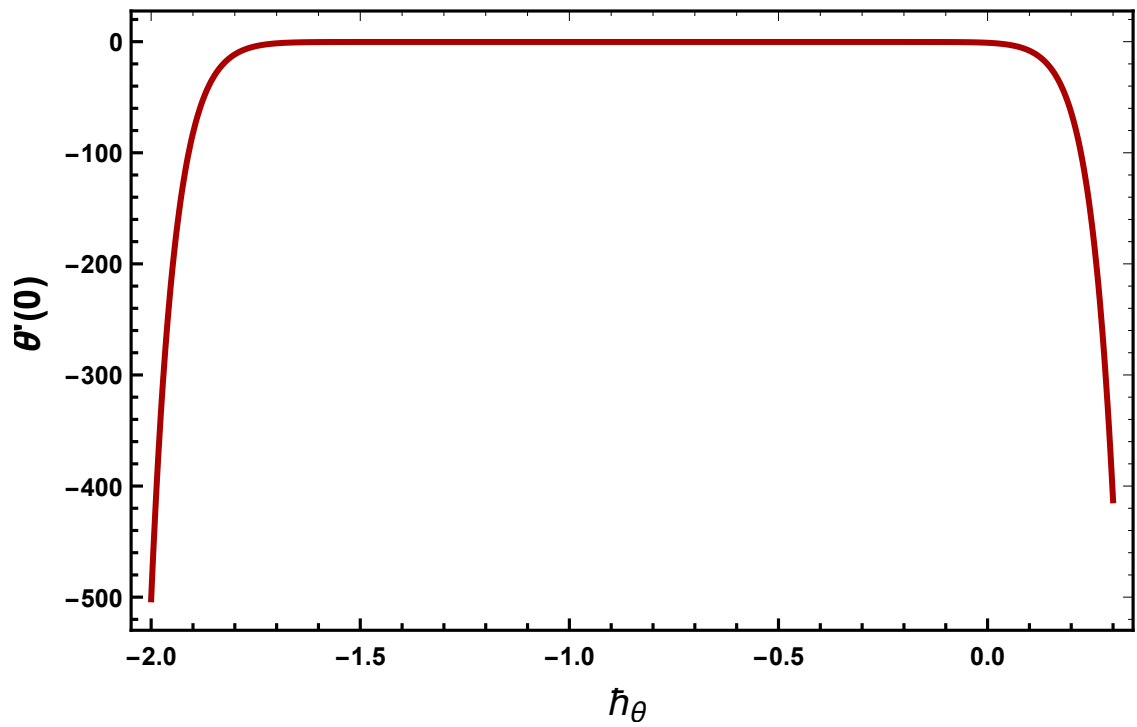
Table 4.1: Series solution convergence for the values $We = 0.1$, $Du = 0.1$, $Sr = 0.1$, $\zeta = 0.1$, $M = 0.1$, $Pr = 0.7$, $Sc = 0.4$, $\theta_w = 1.1$, $Rd = 0.1$, $Gr_T = 0.01$, $Gr_C = 0.01$, $\beta = 0.1$, $\hbar_f = -1.09$, $\hbar_\theta = -0.75$ and $\hbar_\phi = -0.83$.

Approximations	$f''(0)$	$-\theta'(0)$	$-\phi'(0)$
1	-1.1002	0.1857	0.1274
5	-1.1212	0.2687	0.2819
10	-1.1198	0.2643	0.2848
15	-1.1195	0.2646	0.2855
20	-1.1194	0.2651	0.2857
25	-1.1195	0.2654	0.2856
30	-1.1195	0.2654	0.2856
35	-1.1195	0.2654	0.2856
40	-1.1195	0.2654	0.2856

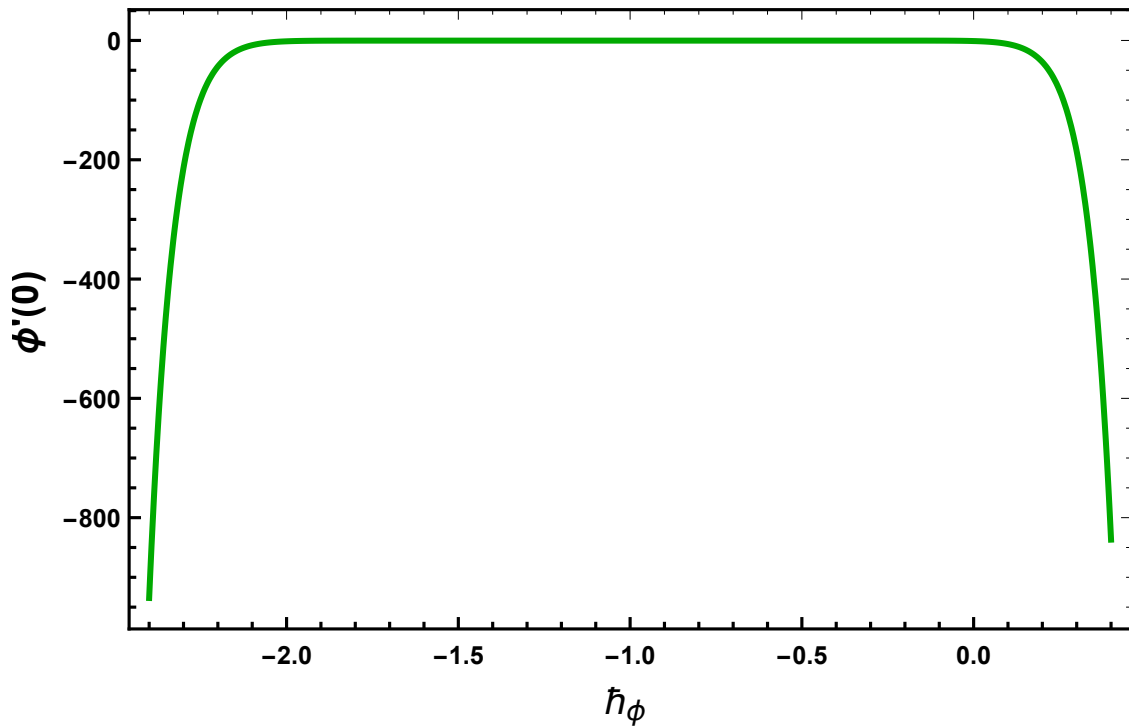
4.5 Result and Discussion

A physical understanding of the Dufour and Soret effect, nonlinear radiation, heat generation, and natural convection movement of the Williamson fluid with heat and mass transfer is carried out. Using HAM, mathematical calculations have been performed, and the effects of relevant parameters are graphically analysed in Figures 4.5-4.17 using Mathematica software. We have taken default parameters values $We = 0.1$, $Du = 0.1$, $Sr = 0.1$, $\zeta = 0.1$, $M = 0.1$, $Pr = 0.7$, $Sc = 0.4$, $\theta_w = 1.1$, $Rd = 0.1$, $Gr_T = 0.01$, $Gr_C = 0.01$, $\beta = 0.1$ for calculation here.

Using all these values graphs and tables are formed otherwise stated. For validity purpose, similarity of the current outcomes of $f''(0)$ with the available published

Figure 4.2: h -curve for $f''(0)$ Figure 4.3: h -curve for $\theta'(0)$

results of Takhar et al. [47] and Yih [62] are explained in Table 4.2. Similarly current outcomes of $\theta'(0)$ equated with the previous published results [135] and [29]

Figure 4.4: h -curve for $\phi'(0)$

are explained in Table 4.3. The results shows great agreement so we are confident that the current results are precise.

There is a dimensionless number called Weissenberg number We that is used in the analysis of viscoelastic flows. Figure 4.5 shows how We varies with velocity profile $f'(\eta)$. Using the dimensionless number, we can compare the viscous forces to elastic forces. Velocity distribution is found to be reduced with an increment in We . It is based on the fact that an increment in We is associated with an increase in fluid relaxation times, creating a resistance to flow. Figure 4.6 explained effect of ζ on $f'(\eta)$. It is noticed that $f'(\eta)$ increases for enhancing values of ζ . Figure 4.7 represents $f'(\eta)$ for the various values of M . It can be noticed that $f'(\eta)$ declined for enhancing M . Figure 4.8 shows the influence of Gr_T on $f'(\eta)$. It can be seen in figure, $f'(\eta)$ increases with raising Gr_T . Also, Gr_C has the same characteristics on $f'(\eta)$ like Gr_T shown in Figure 4.9.

In Figure 4.10, influence of M on $\theta(\eta)$ demonstrated. It can be seen that with raising M , temperature increases. Figure 4.11 highlights the impact of Rd on $\theta(\eta)$. Increase in Rd leads to increase in $\theta(\eta)$, because heat releases from the flow, as Rd raises. Figure 4.12 shows an increment in $\theta(\eta)$ with raising θ_w . Figure 4.13 illustrates Pr on $\theta(\eta)$. We observed reduction in temperature with enhancing Pr . Significance of β on $\theta(\eta)$ is explained in Figure 4.14, where $\theta(\eta)$ enhances with raising β . Figure

4.15 demonstrated significance of Du on $\theta(\eta)$. It can be observed that $\theta(\eta)$ raises with enhancing Du . Figure 4.16 illustrated the impact of Sc on $\phi(\eta)$. It can be seen that $\phi(\eta)$ is declined for larger Sc . Significance of Sc on $\phi(\eta)$ is shown in Figure 4.17, where $\phi(\eta)$ is enhanced with raising Sr . Numerical outcomes of Skin friction coefficient, Nusselt number and Sherwood number are given in Table 4.4.

Table 4.2: Similarity of $f''(0)$ for the various values of M when $We = \zeta = Gr_T = Gr_C = 0.0$.

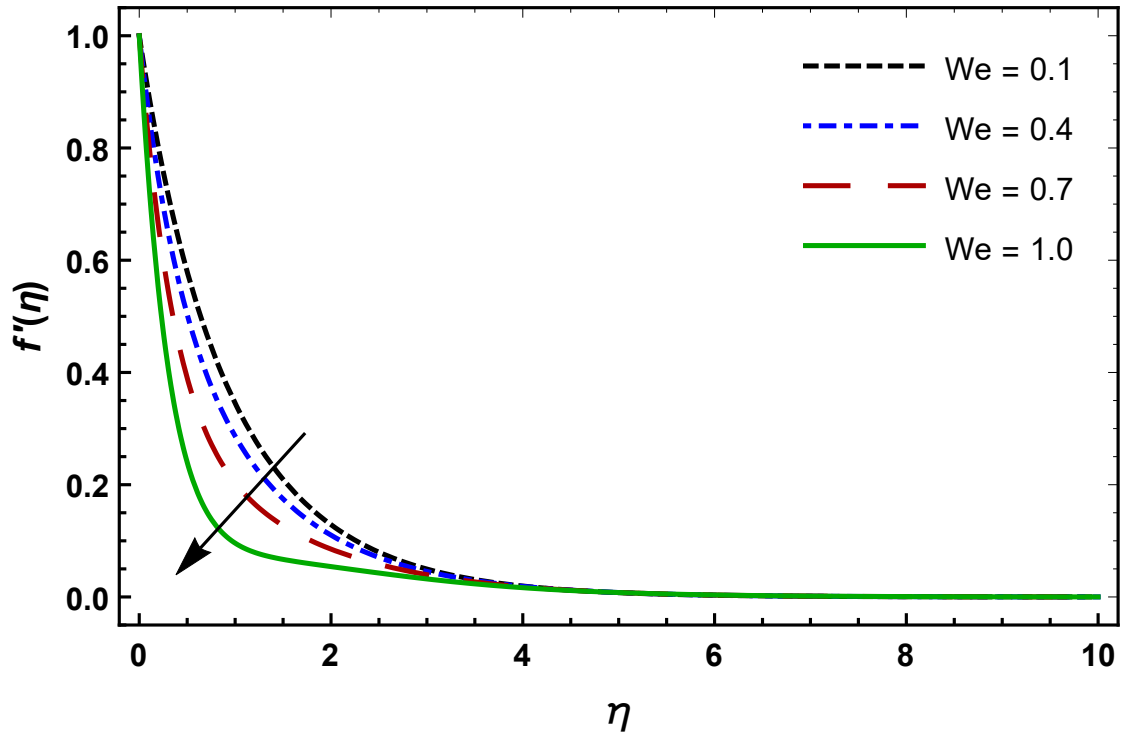
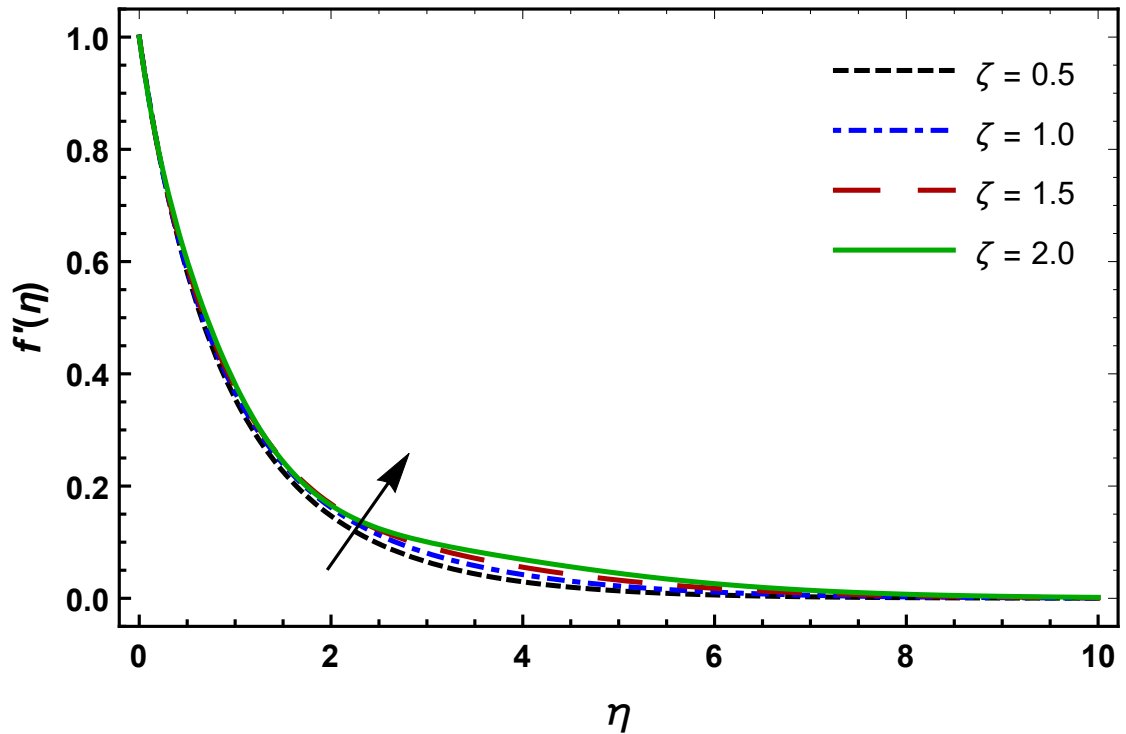
M	Takhar et al. [47]	Yih [62]	Present
0.0	-1.00	-1.0000	-1.0000
0.5	-1.22	-1.2247	-1.2247
1.0	-1.41	-1.4142	-1.4142
1.5	-1.58	-1.5811	-1.5811
2.0	-1.73	-1.7329	-1.7329

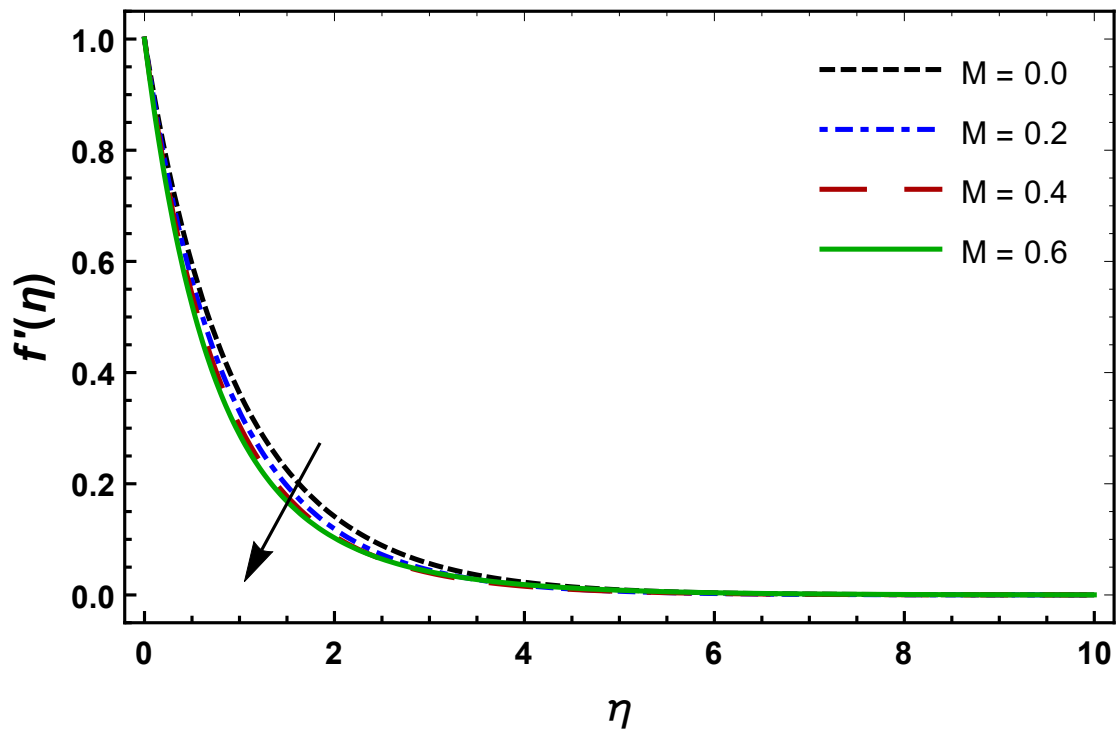
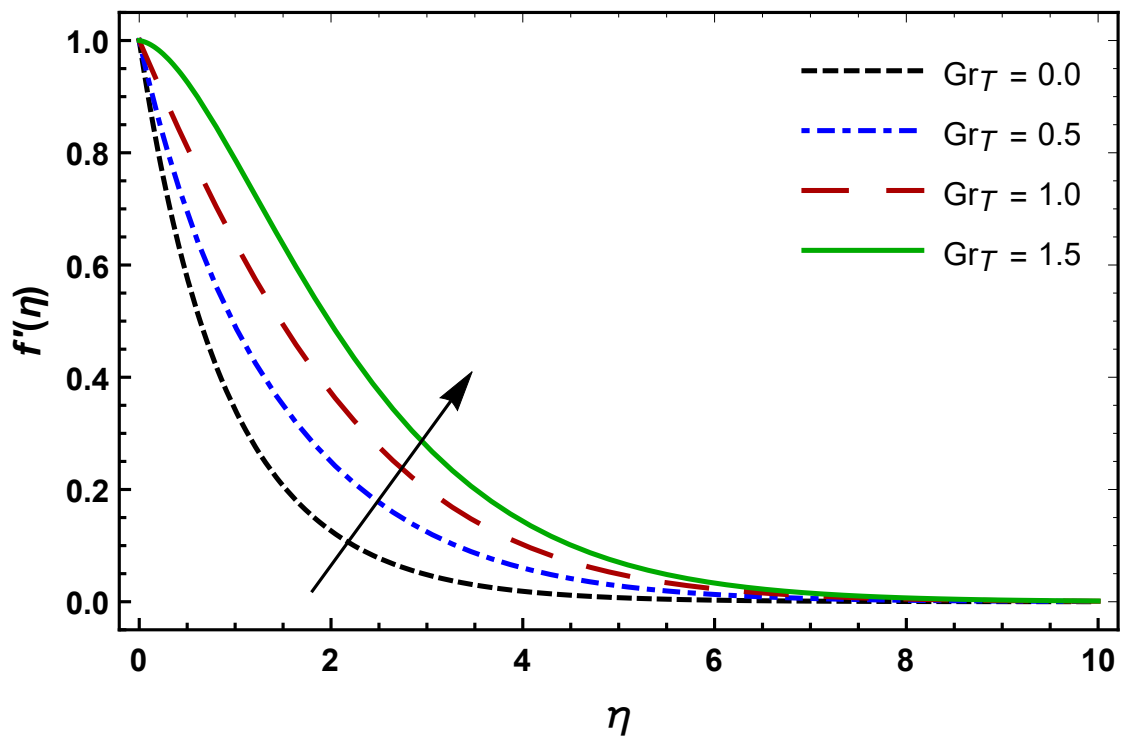
Table 4.3: Similarity of $-\theta'(0)$ for the various values of Pr when $We = Du = \zeta = M = \theta_w = Rd = Gr_T = Gr_C = \beta = 0.0$.

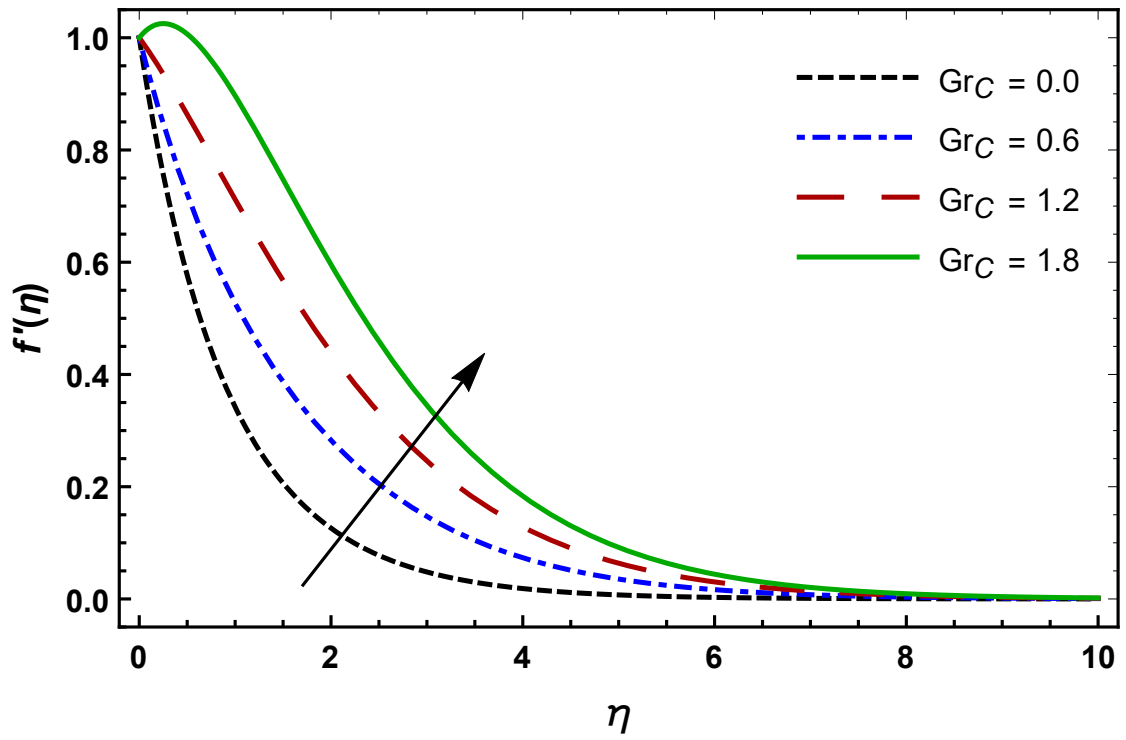
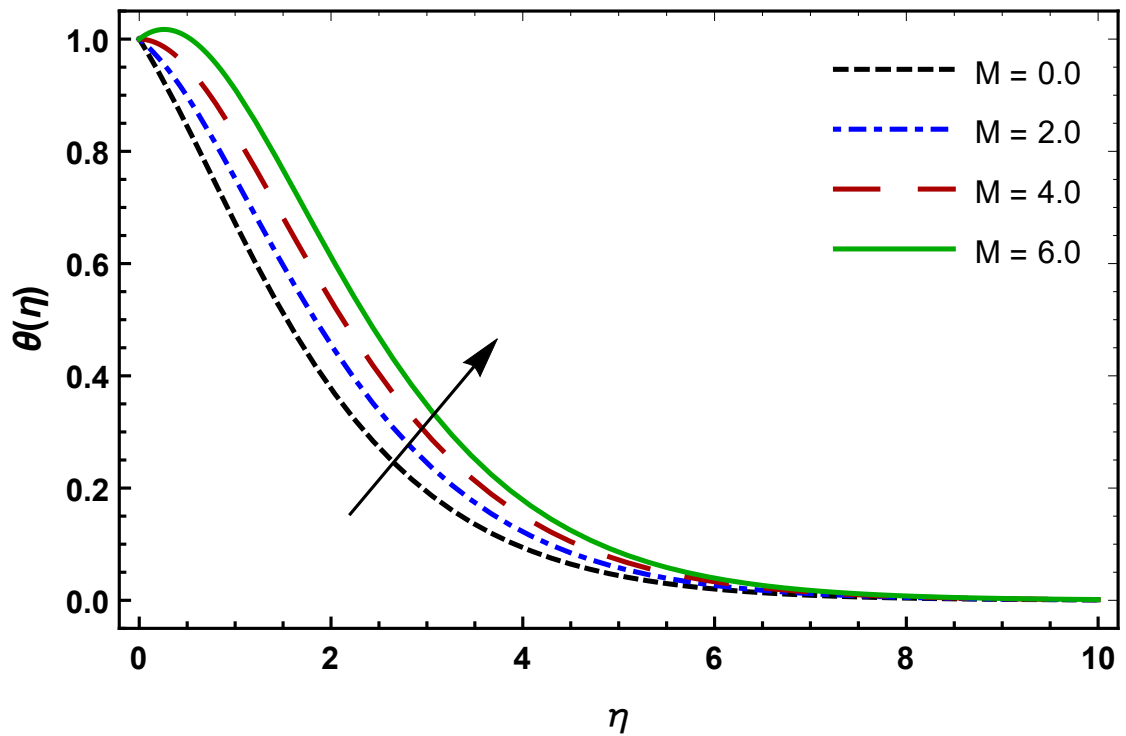
Pr	Khan and Pop [135]	Mabood et al. [29]	Present
0.07	0.0663	0.0668	0.0655
0.2	0.1691	0.1691	0.1691
0.7	0.4539	0.4539	0.4539
2.0	0.9113	0.9113	0.9113
7.0	1.8954	1.8954	1.8954

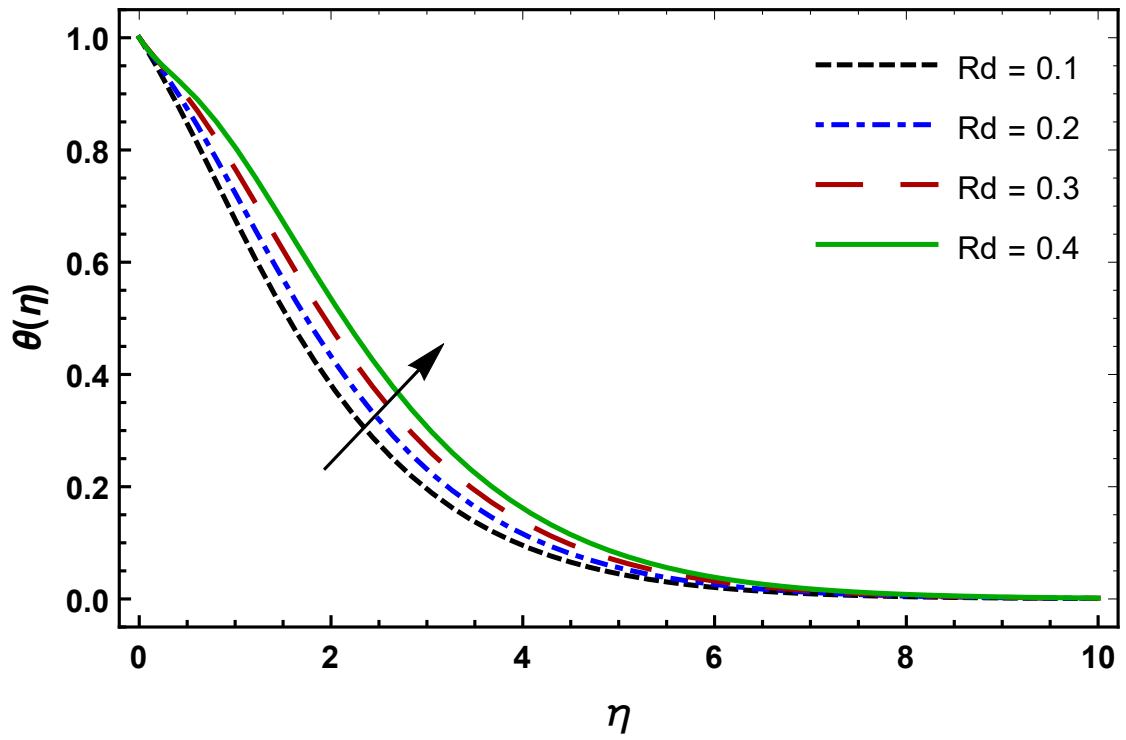
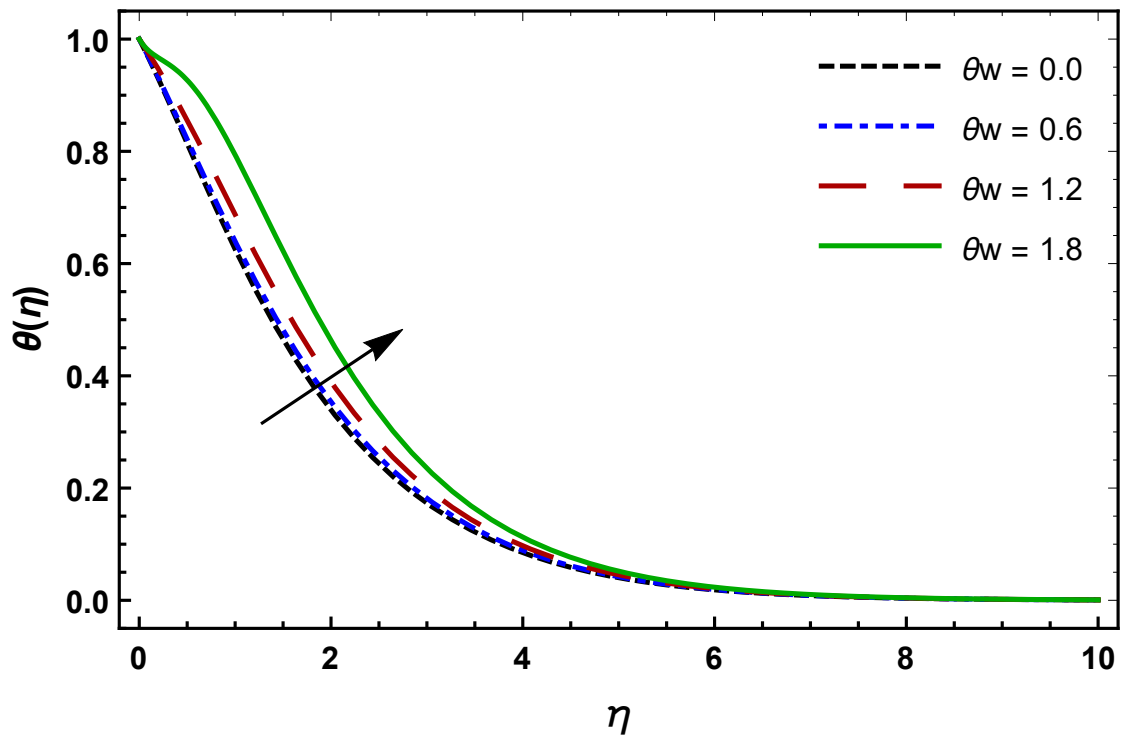
Table 4.4: Skin friction coefficient, Nusselt and Sherwood number for numerous values of $M, \zeta, We, Gr_T, Gr_C, Pr, Rd, Du, \theta_w, \beta, Sc, Sr$.

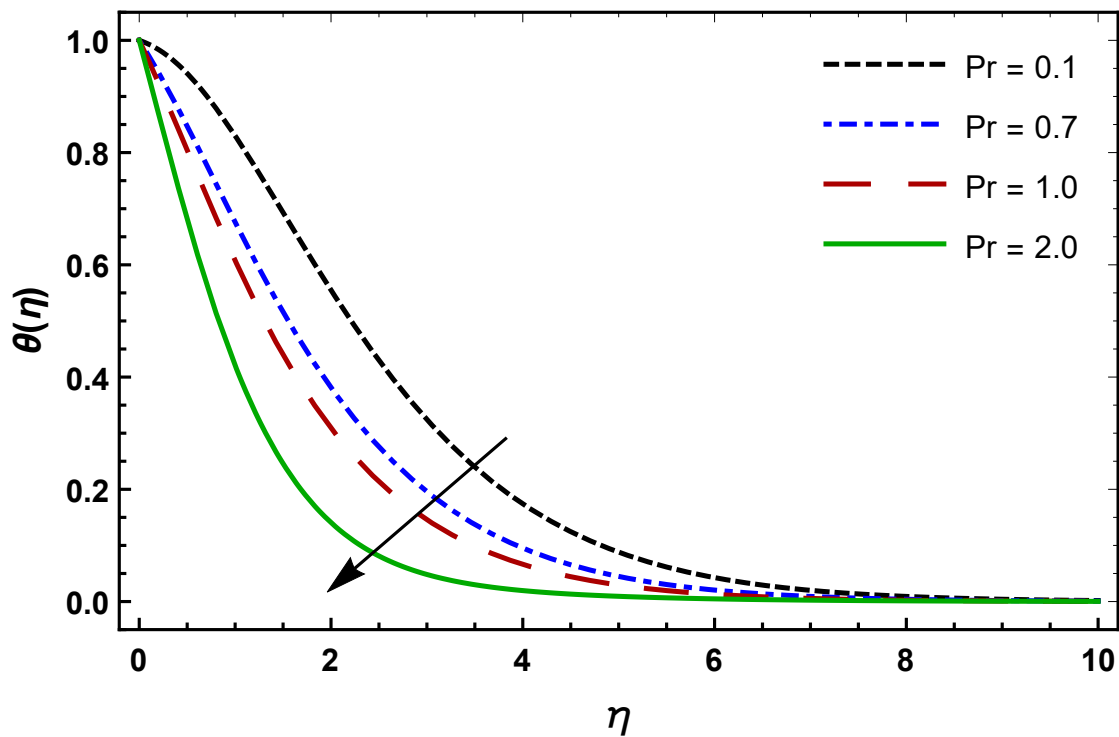
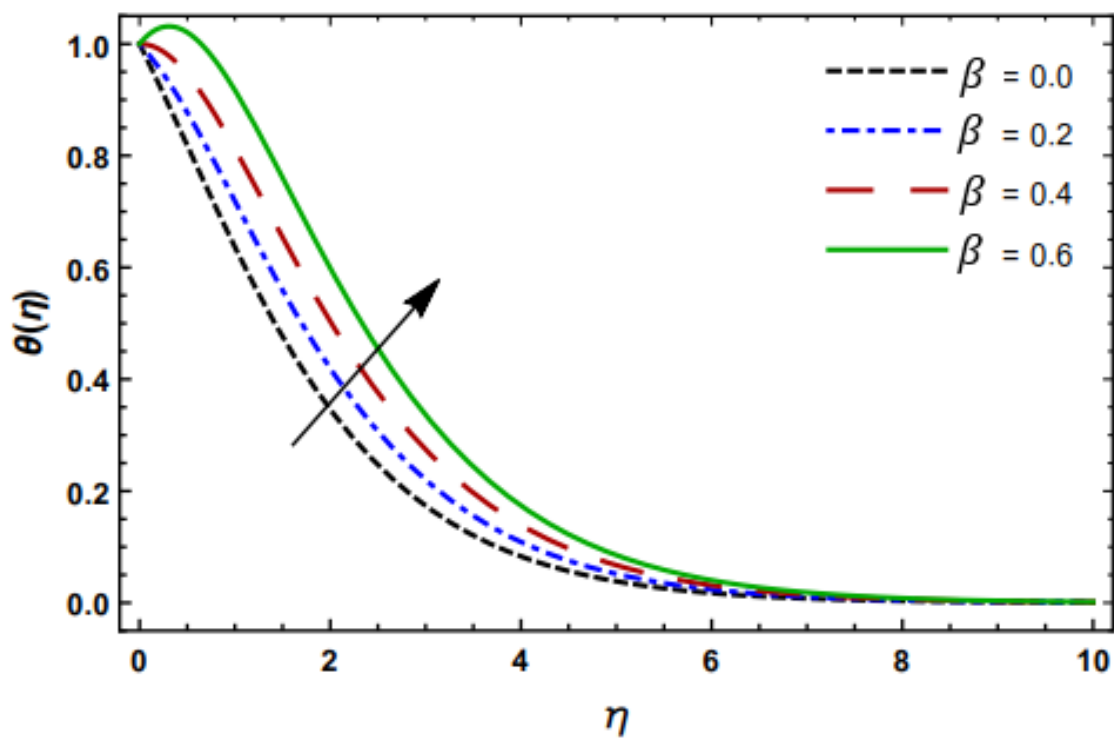
M	ζ	We	Gr_T	Gr_C	Pr	Rd	Du	θ_w	β	Sc	Sr	$C_f Re_x^{1/2}$	$Nu Re_x^{-1/2}$	$Sh Re_x^{-1/2}$
0.1	0.1	0.1	0.01	0.01	7.0	0.1	0.1	1.1	0.1	0.4	0.1	-1.0117	1.4699	0.2056
0.2												-1.0505	1.4690	0.2014
0.3												-1.0875	1.5726	0.1971
	0.2											-1.0337	1.4805	0.2060
	0.3											-1.0555	1.4934	0.2064
		0.2										-0.9278	1.4429	0.2018
		0.3										-0.8001	1.5508	0.1980
			0.02									-1.0104	1.4778	0.2060
			0.03									-1.0092	1.4861	0.2065
				0.02								-1.0064	1.4728	0.2060
				0.03								-1.0010	1.4760	0.2065
					6.0							-1.0087	1.4242	0.2161
					8.0							-1.0147	1.4708	0.1951
						0.2						-1.0106	1.6006	0.2118
						0.3						-1.0094	1.7165	0.2180
							0.2					-1.0069	1.2339	0.2301
							0.3					-1.0021	1.0046	0.2546
								1.2				-1.0115	1.4959	0.2075
								1.3				-1.0112	1.5244	0.2097
									0.2			-1.0069	1.1986	0.2301
									0.3			-1.0021	0.9096	0.2546
										0.5		-1.0118	1.4691	0.2490
										0.6		-1.0119	1.4680	0.2894
											0.2	-1.0117	1.4779	0.1377
											0.3	-1.0116	1.4865	0.0699

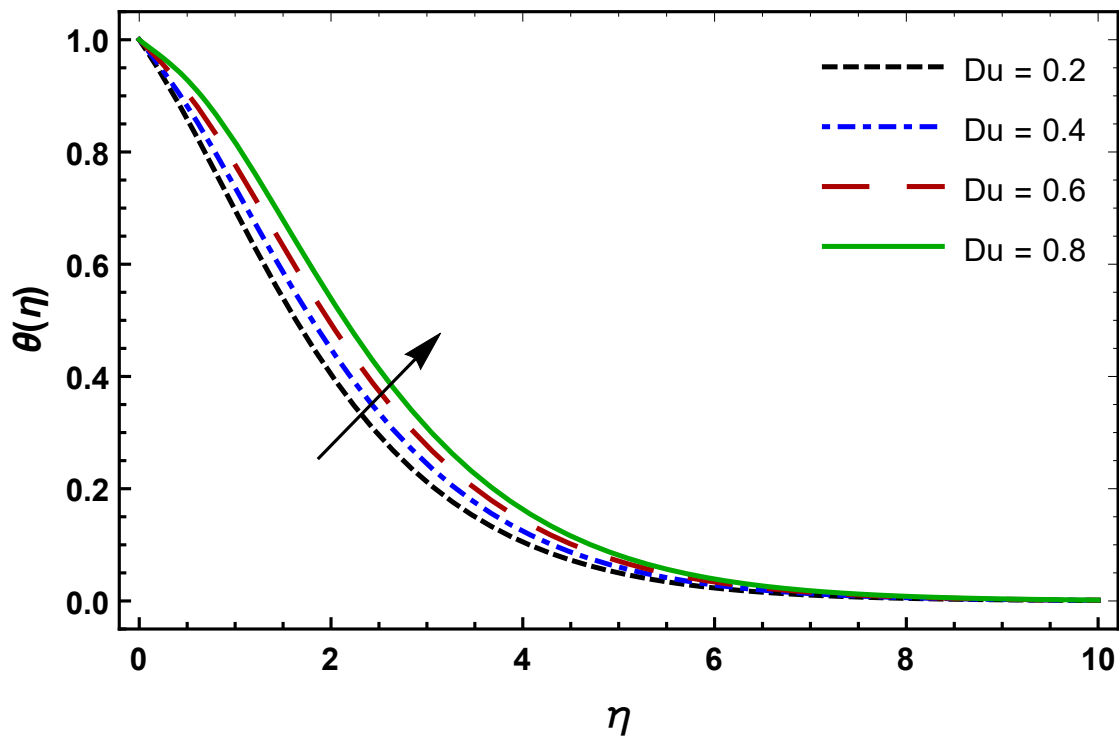
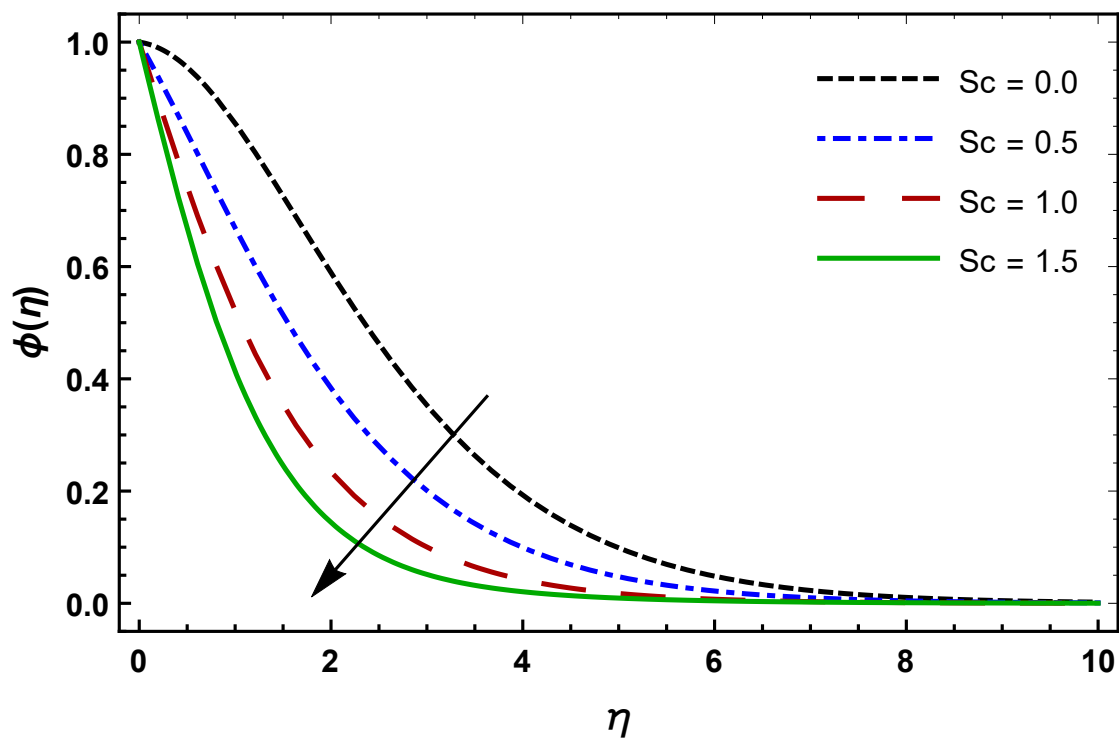
Figure 4.5: $f'(\eta)$ via We Figure 4.6: $f'(\eta)$ via ζ

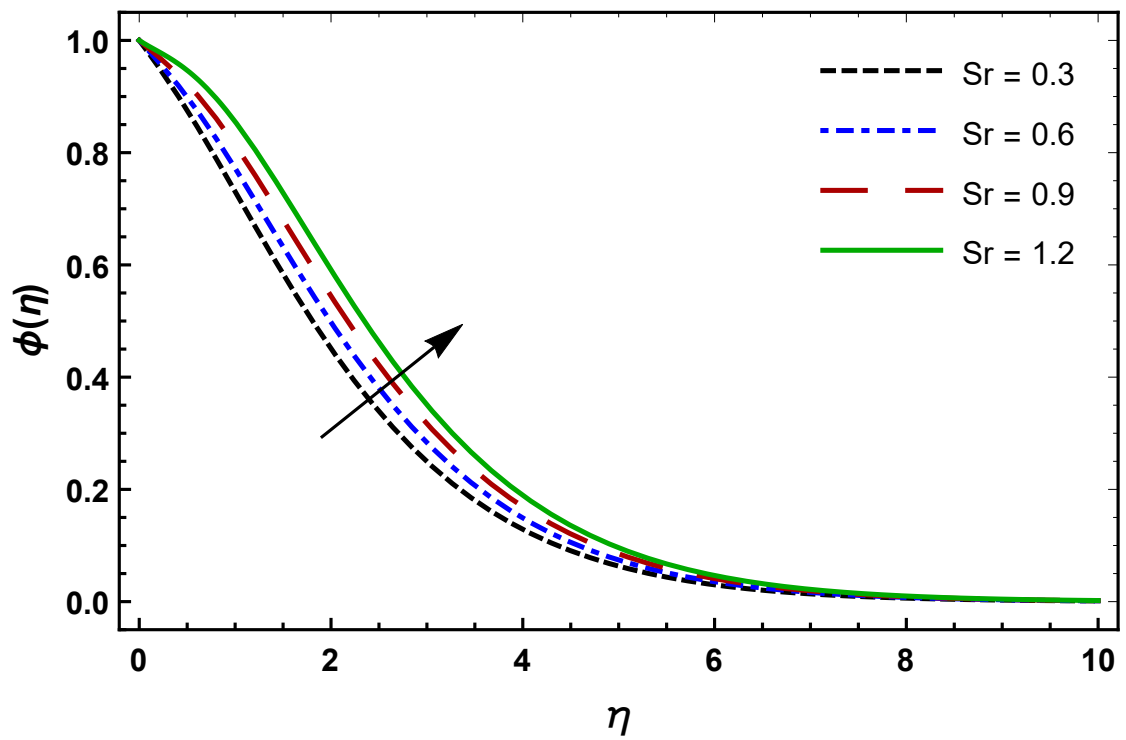
Figure 4.7: $f'(\eta)$ via M Figure 4.8: $f'(\eta)$ via Gr_T

Figure 4.9: $f'(\eta)$ via Gr_C Figure 4.10: $\theta(\eta)$ via M

Figure 4.11: $\theta(\eta)$ via Rd Figure 4.12: $\theta(\eta)$ via θ_w

Figure 4.13: $\theta(\eta)$ via Pr Figure 4.14: $\theta(\eta)$ via β

Figure 4.15: $\theta(\eta)$ via Du Figure 4.16: $\phi(\eta)$ via Sc

Figure 4.17: $\phi(\eta)$ via Sr

4.6 Conclusion

The intention of current research is to explore and compare the combined impacts of temperature dependent viscosity, Soret and Dufour effects on natural convective flow of MHD Williamson fluid past a stretching sheet. The main findings of the research are following:

- We and M reduce velocity profile while Gr_T , Gr_C and ζ behave in opposite way.
- A rise in temperature is observed for M , β , and Du , while a decline is observed for Pr .
- Temperature profile increased for Radiation parameter and temperature ratio parameter.
- Sc and Sr have opposite characteristics according to the concentration profile.
- Skin friction factor is enhanced for We , Gr_T and Gr_C whereas declined for M and ζ .
- Nusselt number is increased for M , Gr_T , Pr , Rd and θ_w while decreased for Du and β .
- Sherwood number is raised for Sc but decayed for Sr .